Investigation of Tapping-Mode Scanning Near-Field Optical Microscope

Yi-ting Huang

Center for the Physics of Materials
Department of Physics. McGill University
Montréal, Canada

A Thesis submitted to the
Faculty of Graduate Studies and Research
In partial fulfillment of the requirements for the degree of
Master of Science

Table of Contents

List of Figures

List of Tables

Abstract

A crucial part of the Scanning Near-Field Microscope (SNOM) is the distance regulation that keeps the separation of a fiber probe tip and the sample surface constant. Previously, shear-force detection was implemented. Shear-force interactions have the disadvantage of being destructive on soft sample. The implementation of an alternative tapping-mode is investigated in this thesis. In tapping-mode, the fiber tip oscillates perpendicularly to the sample surface, thus avoiding the destructive lateral shear-force.

This thesis also provides a general overview of SNOM, including the theory of near-field, the definition of spatial resolution, as well as the tip-sample distance regulation. Tapping-mode feedback is implemented and discussed in comparison to traditional shear-force feedback. Both CD stamper and Polystyrene images were obtained by using tapping-mode SNOM, and compared to images taken under shear-force mode SNOM and Scanning Electron Microscope. Different factors, which affect the performance of tapping-mode SNOM are discussed.

Résumé

Une part cruciale de la microscopie optique à champ proche, ou Scanning Near-Field Optical Microscope (SNOM) est le contrôle de la distance qui maintient la séparation entre l'échantillon et la pointe constante. La détection de force de cisaillement a été réalisée précédemment. L'interaction des forces de cisaillements a l'avantage d'être non-destructive sur des échantillons mous. La réalisation alternative d'un mode *tapping* est étudié dans cette thèse. En mode *tapping*, la pointe en fibre optique oscille perpendiculairement à la surface de l'échantillon, évitant ainsi les forces de cisaillements destructives.

Cette thèse fournie également une vue générale de la technique SNOM, incluant la théorie de champ proche, la définition de la résolution spatiale, ainsi que le contrôle de la séparation entre la pointe et l'échantillon. La boucle de rétro-action du mode *tapping* a été réalisée et est discutée par rapport à celle traditionnelle des forces de cisaillements. La poinçonneuse CD et les images de polystyrène ont toutes deux étés prises sous le mode *tapping* du SNOM et comparés aux images prises par le SNOM en mode force de cisaillement ainsi que la Microscopie Électronique à Balayage. Différents facteurs affectant les performances du SNOM en mode *tapping* sont discutés.

Acknowledgements

I would like to thank my supervisor, Prof. Pete Grütter, who introduced me to the world of nano-science and has guided me from the beginning. His wisdom and patience over the past two years has given me a great support. I would also like to thank Dr. Philip R. LeBlanc for his immeasurable counsel.

This wouldn't has been such a enjoyable project without all of my colleagues in the department. In particular, thanks to Xiaobin Zhu, Mark Roseman, Valentin Yakimov, Kaifeng Liang, Mike Godin, Sun Yan, Vincent Tabard-Cossa, Alex Wlasenko, Benjamin Smith for their assistance. My appreciation also goes to Steve Kecani, Eddie Del Campo, Robert Gagnon, Michel Beauchamp and Frank Van Gils for their help.

Finally, I would like to thank my parents and all of my friends, Manuel Pumarol, Mary Dikeakos, Li Cheng, Pascal Fortin, for their friendship and support.

Chapter 1

Introduction

Since the development of the compound microscope nearly three centuries ago, through the years, technological and scientific studies have required finer and finer resolution. With the techniques of the Scanning Tunneling Microscope (STM), Dieter Pohl *et al.* developed the Scanning Near-Field Optical Microscope (SNOM or NSOM) in 1984. Abbe's barrier (the detectable feature size is restricted to about one-half the wavelength of light) described the diffractio0n limits of conventional far-field microscope. The limits have been surpassed by a new generation of near-field microscope. The placement of an aperture in close proximity to the object has made it possible to deliver high spatial frequency information (evanescent waves) to the detector located in the far distance. This aperture is often fabricated from tapered optical fibers.

In most conventional SNOM, the tip-sample separation regulation is done by using shear forces as a feedback signal. Shear forces are detected by using the fiber probe as a force sensor. The force signal is detected generally by focusing a laser beam onto the fiber and recording the stray light [1]. Several other detection schematics [2,3,4,5,6,7]

employ shear-force feedback; one of the most prominent methods uses a quartz tuning fork [5,8,9], having the fiber tip attached to one of its tines. The tuning fork/probe tip assembly is driven at its resonance frequency and delivers a piezoelectric signal, which is linearly proportional to the fiber amplitude. Both the oscillation amplitude and the phase signals can serve as a feedback signal to control the tip-sample separation when the tip is in close proximity with the sample surface.

An alternative method of distance control for SNOM is to use normal forces "tapping-mode" instead of the lateral shear-force. Tapping-mode is better suited for operating on soft surfaces [10,11], since there are almost no lateral forces involved; i.e., the tip is not dragged over the surface. Lateral forces can not only destroy a soft sample, but also easily break sharp SNOM tips. The latter leads to a degradation of resolution and a reduction in the reliability of SNOM operation.

In Chapter 2, a brief theoretical introduction to near-field imaging is given. Chapter 3 discusses the investigation of tapping-mode SNOM performed during this Thesis, and Chapter 4 draws some conclusions. The major aim of this thesis was to investigate the implementation of tapping-mode SNOM `using a tuning fork detector.

Chapter 2

Scanning Near-Field Optical Microscopy: Theory

This chapter provides background about Scanning Near-Field Optical Microscope (SNOM). In the first section, a theory of high spatial frequency waves (evanescent waves) is introduced. Application of this theory to the optical imaging process provides the connection between the near-field and the far-field; it also helps to define the resolution of conventional microscope and near-field microscope. This will be followed by an example of the two main operation modes and the mechanical properties of the probe tip/tuning fork assembly. At the end, a short introduction to tip-sample distance regulation is given.

2.1 Evanescent Waves

In any plane, a monochromatic electric field can be expressed as [21]:

$$\vec{E}(\vec{R}) = \frac{1}{2\pi} \int d\vec{K}_{x,y} \vec{F}(\vec{K}_{x,y}, z) e^{i(\vec{K}_{x,y} \cdot \vec{r})}, \tag{2.1}$$

where $\vec{K}_{x,y} = (\vec{K}_x, \vec{K}_y)$ is a spatial wave vector parallel to the plane, and $\vec{F}(\vec{K}_{x,y}, z)$ is the Fourier transform of this electric field; $\vec{r} = (x, y)$ is any spatial point in the plane. To satisfy the Helmholtz equation $((\nabla^2 + K^2)\vec{E}(\vec{R}) = 0)$. We get

$$(\frac{d^2}{dz^2} + K_z^2)\vec{F}(\vec{K}_{x,y}, z) = 0, \tag{2.2}$$

where $K_z = (K^2 - K_{x,y}^2)^{\frac{1}{2}}$ (2.3)

The general solution of Eq. (2.2) is:

$$\vec{F}(\vec{K}_{x,y}, z) = \vec{C}(\vec{K}_{x,y})e^{\pm iK_z Z}, \tag{2.4}$$

where $\vec{C}(\vec{K}_{x,y})$ are the functions of $\vec{K}_{x,y}$. The electric field $\vec{E}(\vec{R})$ then becomes:

$$\vec{E}(\vec{R}) = \frac{1}{2\pi}\int\int d\vec{K}_{x,y} C(\vec{K}_{x,y})e^{iK_z Z}e^{i(K_{x,y}\vec{r})}, \tag{2.5}$$

which is a spectrum of plane waves of the form $Ae^{i\vec{K}r}$, where A is the amplitude, $A = \vec{C}(\vec{K}_{x,y})$, and $\vec{K}$ is the wave vectors, $\vec{K} = (\vec{K}_{x,y}, \vec{K}_z)$. From Eq. (2.3), when we have a wave with low spatial frequency (small $K_{x,y}$, K_z is real), it is called a homogeneous wave. On the other hand, when a wave contains high spatial frequencies (large $K_{x,y}$, K_z is imaginary), it is then called an evanescent wave. This type of wave decays exponentially in the z-direction within distances comparable to the wavelength λ. In our SNOM, the object we use is of sub-wavelength size; thus it gives out high spatial frequency information (evanescent waves).

2.2 Near-field and Far-field

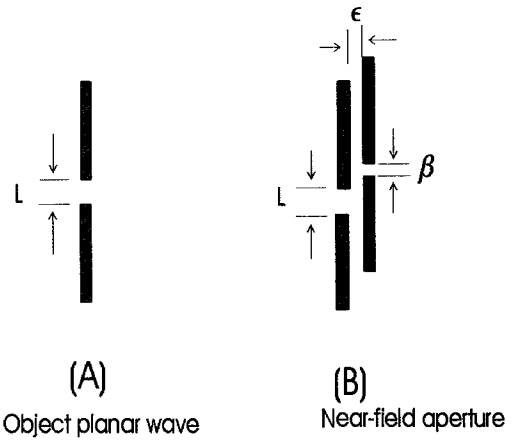

Figure2.1 Model of (a) object of subwavelength slit of width L
(b) a near-field aperture of width β. From [12]

Figure 2.1 shows a simple model [12], which explains how the near-field microscopes overcome the disadvantages of conventional far-field microscopy. The most fundamental issue in SNOM imaging is the ability of delivering high spatial frequency information to the far-field detector. It involves the interaction of the object and the device, which is used to create the image of the object. In Figure 2.1(a), we consider an object with an opening of width L (L is of subwavelength dimensions), located at $z = 0$. A light source with monochromatic plane waves of wavelength λ illuminates this object screen from the left. The field at $z = 0$ is $A(x, z = 0) = E_0 rect(\frac{x}{L})$. A detector (in the image plane) is located in a distance $Z(Z >> \lambda)$ to the right of the object plane. The detected field at far-distance $z = Z$ can be written in terms of the Fourier transform of the field at $z = 0$:

$$A(x, z = Z) = \int_{-\infty}^{+\infty} d\alpha_x \exp(-2\pi i \alpha_x x) F(\alpha_x, z = 0) \exp[-2\pi i (\alpha^2 - \alpha_x^2)^{\frac{1}{2}} Z]. \quad (2.6)$$

Because of the size of the opening (object screen), the diffracted light contains high spatial frequency information (evanescent wave). These waves decays rapidly with z and thus do not survive the journey to the detector $(z = Z >> \lambda)$; only the propagating waves (low spatial frequency) exist in the image plane. So for the far-field Eq.(2.6), we only have to integrate over $|\alpha_x| < \frac{w}{2\pi c}$ (for $(\alpha^2 - \alpha_x^2)^{\frac{1}{2}}$ is positive and real).

This field becomes:

$$A(x, z = Z) = \int_{-w/2\pi c}^{+w/2\pi c} d\alpha_x \exp(-2\pi i \alpha_x x) \frac{\sin \alpha_x L}{\alpha_x} \exp[-2\pi i (\alpha^2 - \alpha_x^2)^{\frac{1}{2}} Z] . \quad (2.7)$$

With the existence of the near-field device (Figure 2.1(b), a subwavelength aperture of width β in a screen at a distance $z = \varepsilon << \lambda$), the field at $z = \varepsilon$ is:

$$A(x, z = \varepsilon) = E_o(x, z = \varepsilon) \times rect(\frac{x}{\beta}).$$

Now we can also define the field at $z = Z$:

$$\begin{aligned} A(x, z = Z) = & \int_{-w/2\pi c}^{+w/2\pi c} d\alpha_x \exp(-2\pi i \alpha_x x) \exp[-2\pi i (\alpha^2 - \alpha_x^2)^{\frac{1}{2}} (Z - \varepsilon) \\ & \times \int_{-\infty}^{+\infty} d\alpha_x \exp(-2\pi i \alpha_x' \varepsilon) F(\alpha_x', z = 0) \frac{\sin(\alpha_x - \alpha_x')L}{\alpha_x - \alpha_x'} \exp[-2\pi i (\alpha^2 - \alpha_x^2)^{\frac{1}{2}} \varepsilon] \end{aligned} \quad (2.8)$$

Eq.(2.7) and Eq.(2.8) are the two equations which represent the field at a distance of $z = Z$ in the presence of the near-field aperture (2.8) and without the presence of the aperture (2.7). We can examine whether the high spatial frequency information can be detected by a detector at $z = Z$ by considering one specific frequency ϖ (putting $F(\alpha_x, z = 0) = F\delta(\alpha_x - \varpi)$ in both formulas (2.7) and (2.8)).

For the conventional far-field microscope, only low frequency can survive at macroscopic distances $z = Z$:

$$A((x, z = Z) = E_o \exp(-2\pi i \varpi x) \exp[-2\pi i(\alpha^2 - \varpi^2)^{\frac{1}{2}} Z] \qquad \text{for } \varpi < \frac{w}{c} \tag{2.9}$$

and $= 0$ for $\varpi > \frac{w}{c}$

While for the case with the near-field aperture:

$$\begin{aligned} &A(x, z = Z) = E_o \exp[-2\pi i(\alpha^2 - \varpi^2)^{\frac{1}{2}} \varepsilon] \\ &\times \int_{-w/2\pi}^{+w/2\pi} d\alpha_x \exp(-2\pi i \alpha_x x) \exp[-2\pi i(\alpha^2 - \alpha_x^2)^{\frac{1}{2}} (Z - \varepsilon)] \frac{\sin(\alpha_x - \varpi)L}{\alpha_x - \varpi} \end{aligned} \tag{2.10}$$

The high spatial information gets delivered to the far-field detector. This explains why the presence of an aperture of sub-wavelength dimensions in the near-field of an object can help to deliver high spatial frequency information by converting the evanescent waves into propagating waves, thus making the detection possible.

2.3 Spatial Resolution

Spatial resolution has always been the central issue related to the performance and the sensitivity of an optical microscope. For the conventional optical microscope, the spatial resolution limit is imposed by the wave nature of light (Abbe's barrier). The requirement of better resolution is the driving force behind the development of the near-field microscopy.

2.3.1 Classical Resolution Limits

We assume a sample lies in a $z = 0$ plane $(x, y, 0)$ with an electric field of $\vec{E}(x, y, 0)$. The Fourier spectrum of that field is:

$$\vec{F}(\vec{K}_{x,y}, z = 0) = \vec{F}(\vec{K}_{x,y}). \tag{2.11}$$

Assuming that a detector is located in a distance L in the z-direction, from Eq.(2.11) with the boundary condition $\vec{F}(\vec{K}_{x,y}, z \to \infty) = 0$, we get:

$$\vec{F}(\vec{K}_{x,y}, L) = \vec{F}(\vec{K}_{x,y}) e^{iK_z L}. \tag{2.12}$$

Eq.(2.12) shows that we can calculate the Fourier spectrum at any distance in the z-direction by simply multiplying the $z = 0$ Fourier spectrum with the factor $e^{iK_z L}$, where L is any distance in the z-direction. From Eq.(2.3), we know K_z can be both real $(K_{x,y}^2 << K^2)$ and imaginary $(K_{x,y}^2 >> K^2)$. In the former case, the corresponding Fourier spectrum are propagating waves with features larger than $\frac{\lambda}{2\pi} = \frac{1}{K}$. This is the low spatial frequency wave, which will make it to the far-field image plane.

From the above considerations, we know that for conventional far-field microscope, the resolution limit (the smallest feature that can be detected) is:

$\Delta d = \frac{1}{K} = \frac{\lambda}{2\pi}$, which agrees with the Abbe's criterion $\Delta X_{\min} = \frac{1.22\lambda}{2n} \sin\varphi$,

where n is the index of refraction of the medium between the object and the lens, and φ is the aperture angle in the medium. For a conventional optical microscope –

a system whose objects, probes, and separations are large with respect to the wavelength of light – the resolution is only slightly smaller than the wavelength of the light source.

2.3.2 SNOM Resolution

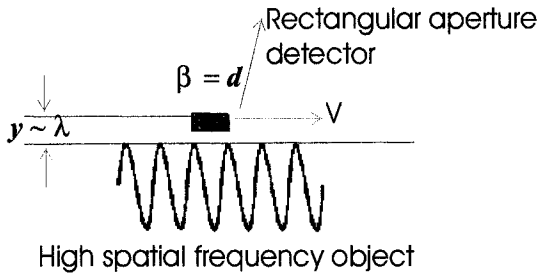

Figure 2.2 A schematic of a small aperture scanning over a high spatial frequency object

Recall from the previous discussion of how a small device helps the high spatial frequency information get delivered to the far-distance detector. A small aperture is brought into the near-field of the object. The following discussion explains how the dimensions of the aperture affect the spatial resolution. Consider an object of high spatial frequency α, described by $a(x) = 1 + \cos(2\pi\alpha x)$, as depicted in Figure 2.2. A rectangular aperture detector of size β, scanning at a velocity v, is in close proximity to the object. The detected signal is [12]:

$$G(x) = D\int_{-\infty}^{+\infty} a(x)\,rect(\frac{x}{\beta})dx, \tag{2.13}$$

where D is the detector response.

With the conversion of spatial frequencies to temporal frequencies ($f = \alpha v$), we get:

$$G(x) = D\int_{-\infty}^{+\infty} a(x)rect(\frac{x}{\beta})dx$$

$$= D\int_{-\frac{\beta}{2}}^{+\frac{\beta}{2}}[1+\mathrm{Re}\{e^{2\pi i}(ft-\alpha x)\}]dx \qquad (2.14)$$

$$= \beta D + \frac{D}{\pi\alpha}\sin(\pi\alpha\beta)\cos(2\pi ft)$$

To maximize this detected signal $G(x)$, the aperture size must be of the order of the sample size.

$$\beta = \frac{1}{2\alpha} = \frac{v}{2f} = d, \qquad (2.15)$$

where d is the sample spacing size ($d = \frac{\lambda}{2\theta} = \frac{\lambda}{2(\alpha\lambda)} = \frac{1}{2\alpha}$)

In order to have the highest possible resolution, we must use an aperture in the near-field of the sample with a size comparable to the sample spacing size.

2.4 Modes of Operation

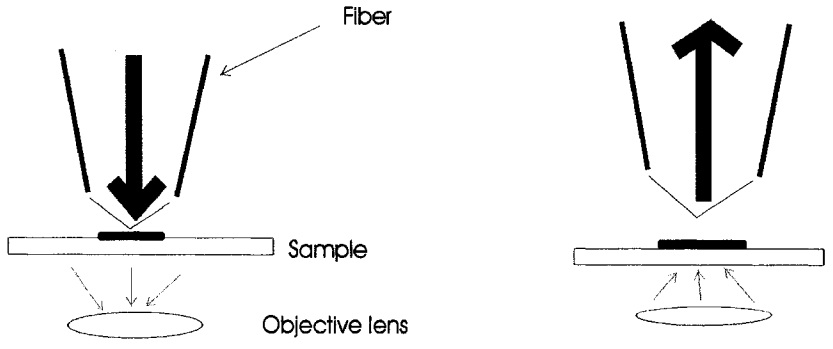

(A) Illumination mode (B) Collection mode

Figure 2.3 Two main SNOM operation modes

Figure 2.3 depicts the two main operation modes of SNOM in (a) illumination mode and (b) collection mode [13]. A detailed discussion on these two operation modes has to involve the imaging process. Supposed matrix M represents the intrinsic properties of the object. The only two fields involved in SNOM imaging are those of the tip (E_{tip}) and of an objective lens (E_{lens}). M, E_{tip} and E_{lens} are functions of position (r), wavelength (λ) and time (t).

In illumination mode, the probe aperture acts as a light source and the interaction between the probe tip and the object defines an available field $(E_{tip} \bullet M)$. While in collection mode, light is collected through the probe aperture, and the available field is $(E_{lens} \bullet M)$. After the imaging operation, a signal of image ($I(r, \lambda, t)$) can be written in terms of the interaction between M, E_{tip} and E_{lens}:

$$I(r, \lambda, t) = \int\int_{\lambda}\int E_{tip} \bullet M \bullet E_{lens} dr d\lambda dt \tag{2.16}$$

2.5 Mechanical Properties of Tuning Fork/Fiber Probe Assembly

2.5.1 Optical Probe

An optical fiber can be considered as an oscillating beam of diameter α with one side clamped to the tuning fork tine. The differential equation is given by:

$$EI\frac{\partial^4 z}{\partial y^4} = -(d\frac{\partial^2 z}{\partial t^2} + \gamma\frac{\partial z}{\partial t}), \tag{2.17}$$

where E is the Young's modulus ($E = 79GPa$ for quartz material [14]), $I = \frac{\pi\alpha^4}{4}$ - the moment of area around the beam axis, d is the mass per unit length, and γ is a damping parameter.

The damping mainly comes from both the internal damping of the material γ_1, and the shear-force damping, which depends on the tip-sample distance D, and affects only the tip $(y = M)$. So we get:

$$\gamma = \gamma_1 + \gamma_2(D)\delta(y - M) \tag{2.18}$$

Firstly, we consider a freely oscillating beam $(\gamma = 0)$, from Eq.(2.17), we get

$$\frac{d^4 z(y)}{dy^4} = \kappa^4 z(y) \ , \tag{2.19}$$

where $\kappa^4 = \frac{w^2 d}{EI}$, by assuming z has the form $z(y,t) = z(y)e^{iwt}$. The general solution for Eq.(2.19) is:

$$z(y) = \beta_1 \cos(\kappa y) + \beta_2 \cosh(\kappa y) + \beta_3 \sin(\kappa y) + \beta_4 \sinh(\kappa y) \tag{2.20}$$

With the boundary conditions:

$$z(0) = z'(0) = z''(M) = z'''(M) = 0$$

We get:

$$\cos(\kappa M)\cosh(\kappa M) + 1 = 0 .$$

The first three numerical solutions of Eq.(2.20) and the corresponding resonance frequencies for an optical fiber with an extension of 1 millimeter from the gluing point on the tuning fork are shown in Table 2.1.

κM	$f(\frac{w}{2\pi}, kHz)$
1.875	37.184
4.694	58.853
7.855	76.109

Table 2.1 The first three values of κM and the corresponding resonance frequencies for a fiber with an extension of 1 millimeter from the edge of the tuning fork, from [14]

2.5.2 Tuning Fork /Fiber Probe Assembly

A quartz tuning fork is used as an interaction force transducer. It is driven at its resonance frequency. Each tine of the tuning fork can be thought of as an oscillator, with constant K_{stat}, oscillating with small amplitude $\alpha(t)$. The equation of motion for such an oscillator driven at frequency w is:

$$m_0 \frac{\partial^2 \alpha}{\partial t^2} + F_D + K_{stat}\alpha = F \exp(iwt), \tag{2.21}$$

where m_o is an effective mass and F is the mechanical drive force exerted by the piezo dither, and w is the driving frequency. We assume F_D represents the sum of the drag forces, which, in SNOM, results from the tip-sample shear-force interaction. It can be expressed as:

$F_D = m_o \gamma \frac{\partial \alpha}{\partial t}$ (γ is a damping parameter with the unit of frequency).

The solution to Eq.(2.21) is:

$$\alpha(t) = \frac{e^{iwt}(F/m_o)}{w_o^2 - w^2 + i\gamma w}, \tag{2.22}$$

where w_o is the resonance frequency of the tuning fork, which is defined as $w_o = (\frac{K_{stat}}{m_o})^{\frac{1}{2}}$.

When the tuning fork is driven right at it resonance frequency $(w = w_o)$, we get the amplitude $\alpha_o = \frac{e^{iW_o t}(F/m_o)}{i\gamma w_o}$. With the definition of the mechanical Q-factor of the tuning fork (Q factor, defined as $w_o / \Delta w_{FMHM}$, with Δw_{FMHM} being the full width of the resonance peak at half maximum, and $f_o = \frac{w_o}{2\pi}$), we can finally get the oscillation amplitude and the shear-force experienced by the tuning fork [8]:

$$\alpha_o = [\frac{\sqrt{3}Q}{iK_{stat}}]F \tag{2.23}$$

$$F_{DO} = i(\frac{K_{stat}}{\sqrt{3}Q})\alpha_o \tag{2.24}$$

(α_o and F_{Do} are 90^o out of phase with regard to the driving force).

From Eq.(2.24), we can see that this is a spring equation with effective spring constant $K_o = \frac{K_{stat}}{\sqrt{3}Q}$. Experimentally, we usually obtained a Q factor of around 350 (with an attached fiber), so the effective spring constant is around 43 N/m, which demonstrates how the stiff tines of a tuning fork can be made dynamically softer. When a tuning fork is driven at or near its resonance frequency, the oscillating amplitude of the two

tines is at a maximum. Figure 2.4 is a typical resonance peak of a tuning fork with Q factor of around 5,000 (bare tuning fork, no fiber tip).

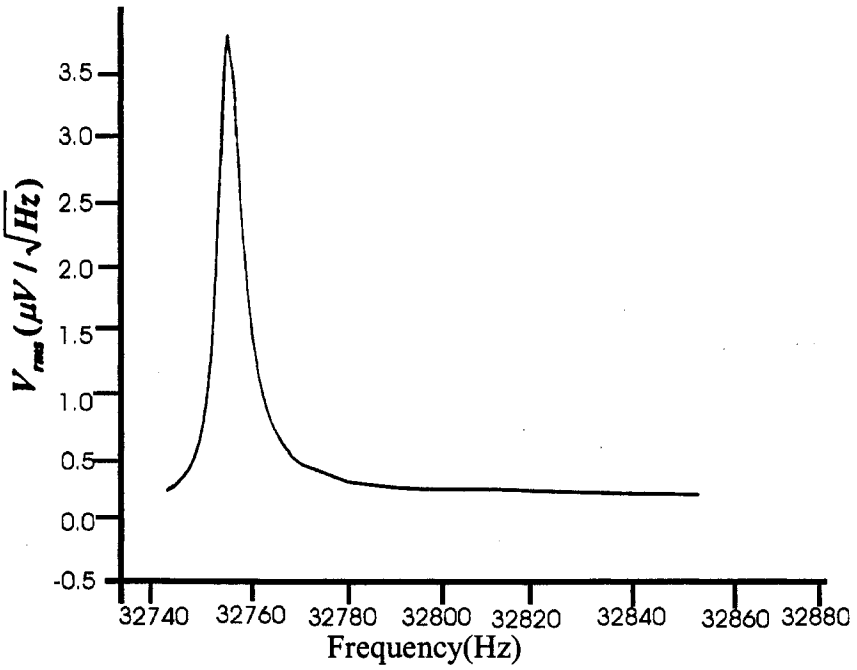

Figure 2.4 Resonance frequency peak for bare tuning fork (Q~5,000)

The Q factor is an essential factor relating to the performance of the SNOM. The thermally limited minimum detectable force gradient using an AC AFM driven at the cantilever resonance is given as [22]:

$$F'_{\min} = \frac{1}{A}\frac{\sqrt{4K_{stat}K_B TB}}{w_o Q}, \tag{2.25}$$

where A is the oscillation amplitude of the probe assembly, and B is the detection bandwidth. Therefore, high sensitivity requires a high Q factor. In tapping mode SNOM, we have $A \cong 20nm$, $K_{stat} = 26\times10^3 N/m$, and $B = 260Hz$, we thus get $F'_{\min} = 5.6\times10^{-3} N/m$.

When a fiber is attached to one of a tuning fork's tines, the Q factor of the assembly can be dramatically reduced. The Q factor of a tuning fork/probe tip assembly is essentially dependent on the symmetry of both of the tuning fork's tines. When the two tines are not strictly equivalent, a mismatch Δf of the resonance frequencies between its two tines will result. In Ref. [15], the effect of the tine asymmetry on the Q factor was tested. The inverse Q factor of a tuning fork as a function of Δf is plotted and the line of best fit found to be:

$$\frac{1}{Q} = \frac{1}{Q_o} + \alpha \Delta f^2, \tag{2.26}$$

where Q_o is the quality factor of bare tuning fork (~5,000) and α is a fitting parameter. Experimentally, it was found that for a typical tuning fork, $\alpha = 1.8 \times 10^{-9}$. This mismatch Δf is dependent on the extra mass and stiffness due to the attachment of a fiber probe to only one of its tines. It is given by:

$$\frac{\Delta f}{f} = \frac{1}{2}\left(\frac{\Delta K}{K} - \frac{\Delta M}{M}\right). \tag{2.27}$$

Here ΔK and ΔM represent the changes in the effective spring constant and the effective mass of the tine. In Section 3.2, we will further discuss how two different configurations – shear-force mode and tapping-mode – affect the Q factor.

2.6 Feedback Distance Regulation

As shown in Section 2.2, a SNOM probe essentially converts an exponentially decaying wave into a signal detectable in the far field. The amount of light collected by the probe depends exponentially on the tip-sample separation, which thus needs to be maintained constant. To control the distance between the tip and the sample, one usually measures the interaction force between tip and sample. A feedback circuit identical to that of an atomic force microscope (AFM) is generally used to maintain the interaction force constant. An implicit assumption is made that maintaining the interaction force constant keeps the tip-sample interaction constant. Various AFM operation modes can be implemented with a tapered SNOM fiber tip. The most common force interaction used is shear force, where the fiber tip is oscillated parallel to the sample surface. This works and has been implemented in our SNOM [14] but can lead to lateral forces large enough to destroy fragile (biological) samples or very sharp probe tips. An alternative is to use tapping mode [2,16,17,18,19], where the tip is oscillated perpendicularly to the surface. The aim of this thesis is to investigate the implementation of tapping mode distance control in our SNOM, as this would possibly lead to a more reliable and less destructive routine operation.

Chapter 3

Instrumentation

Figure 3.1 shows a schematic of our Scanning Near-Field Optical Microscope (SNOM [14]). All SNOM components are secured to a workstation which shields the microscope from external vibrations (the most significant external vibrations are building vibrations of frequencies below $100\ Hz$). We use a Helium-Cadmium laser, which can provide 442-nanometer wavelength (blue light) and 325-nanometer wavelength (ultraviolet light) simultaneously. A quartz tuning fork is implemented to detect the oscillations of the fiber probe. A fiber probe with a tapered end is glued to one of tuning fork's tines (with a cyanoacrylate glue). The whole tuning fork/probe tip assembly sits inside a piezoelectric sample scanner tube, the z-portion of which is controlled by a feedback controller maintaining the interaction force constant. While acquiring data, the sample scanner is scanned with respect to the fixed probe tip. The sample is mounted onto a thin (0.17 mm) glass coverslip, which is held (by Samarium-Cobalt magnets) in the end of the sample scanner tube.

3.1 Optical Fiber Probe

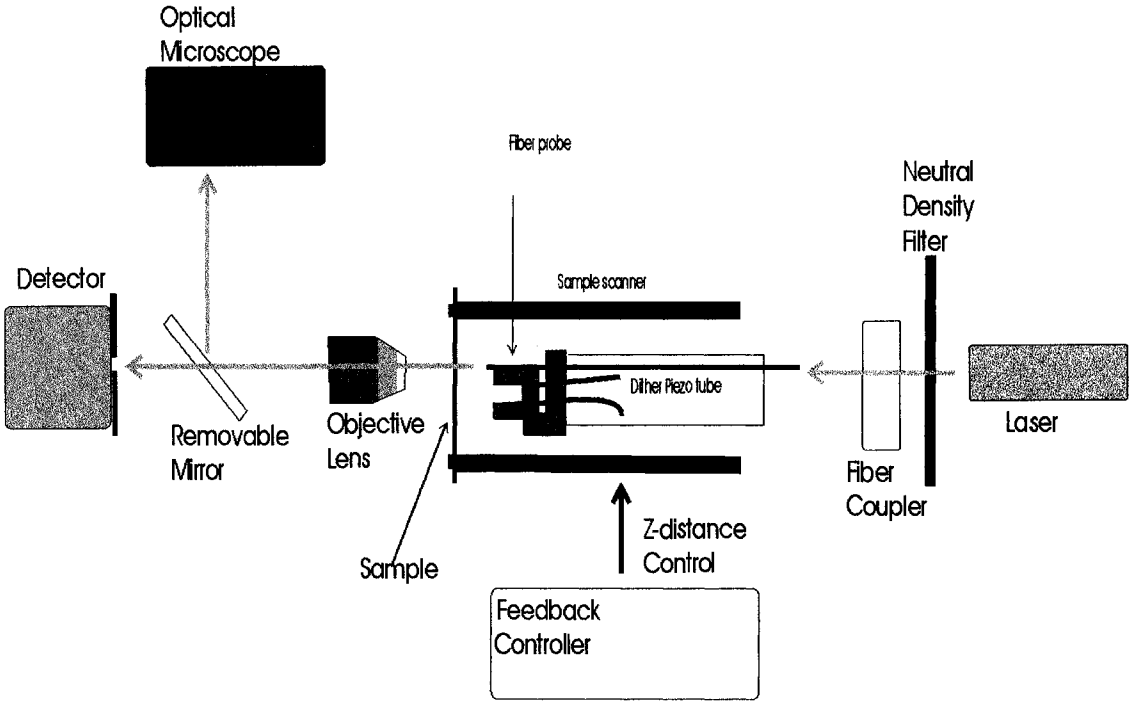

Figure 3.1 A schematic of Scanning Near-Field Optical Microscope

3.1.1 Manufacturing of Tapered Fiber Probes

A 3M single-mode fiber with an operating wavelength of 630 nm and a cutoff wavelength of 620 nm is used. It has a core diameter of 3.3 microns, a cladding diameter of 125 microns and an acrylate jacket diameter of 250 microns. The end of the optical fiber was tapered by using either a micropipette puller or chemical etching. The puller uses a hand-made Platinum-Iridium coil of wire as a heating filament. The heating-and pulling process includes two steps:

a. at some temperature T_h, the pulling and rupture of a heated fiber.

b. cooling and relaxation until viscous flow is negligible.

All the pulling parameters, including the heating filaments current, the pulling strength, the fiber velocity at which the pulling force is exerted, need to be readjusted every time a new filament is used.

An alternative method for creating tapered probe tips involves a chemical etching processes. We used about 100 mL of a 40% HF solution in a petri dish covered by 50 mL of 1-octanethiol (to prevent HF from evaporation). Fibers were immersed in the solution for about one hour, and then we dip the etched fibers into dichloromethane for 25 seconds to strip the fibers off their protective jackets. This method creates the desired taper shape and tip size of the fiber.

Once the taper region of the fiber is done, an aperture has to be properly defined to make the SNOM probe. When light is coupled into fiber, it will travel down to a point in the taper region where the fiber diameter cannot maintain the propagating wave any longer. This light will leak out from the fiber. The leaking of light will create an aperture much greater than the desired aperture. To have a smaller aperture, an Aluminum metal coating is deposited on the taper region by physical vapor deposition (PVD) processes [14] to create aperture of ~ 50nm in size. Figure 3.2 is a schematic illustration of PVD. The fibers are usually tilted by 15^0 with respect to the direction of evaporation, thus the aluminum metal coating will covers only the tapered region but not the tip.

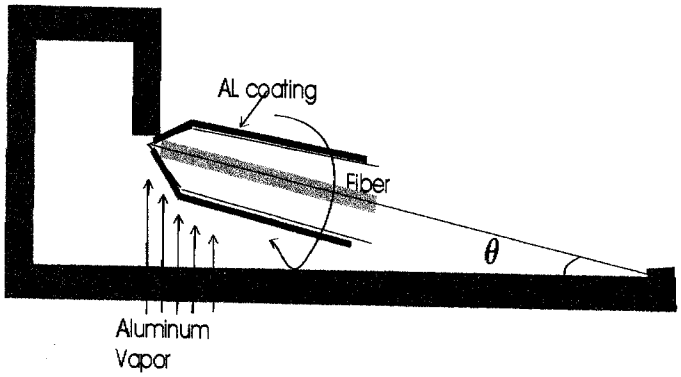

Figure 3.2 Physical vapor deposition (PVD) of aluminum onto fiber probes. From [14]

3.1.2 Tuning Fork/Fiber Probe Assembly

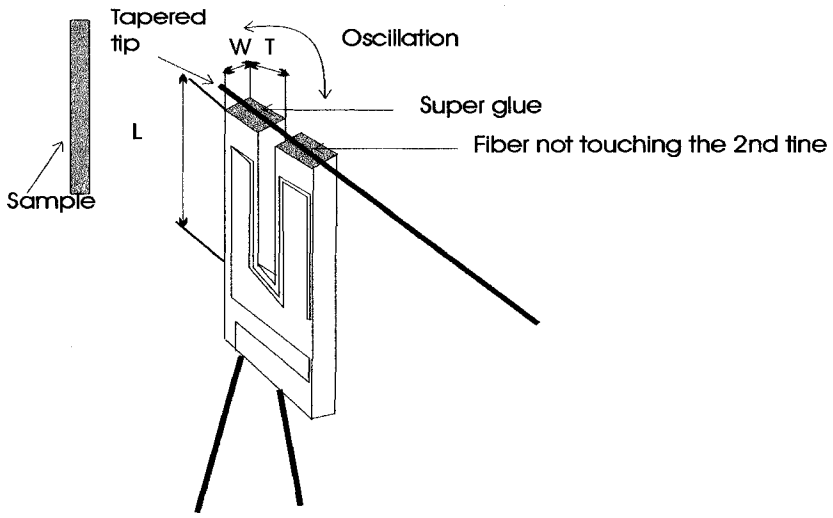

Figure 3.3 Tuning fork/probe tip assembly of tapping-mode SNOM

Central to force and force gradient detection in AFM is a deflection sensor. In most AFMs and SNOMs this is achieved optically. In SNOM this has the potential to interfere with the optical signal. It is for this reason that our deflection detection system was implemented with piezoelectric detection by using quartz tuning forks as the sensing element. Enhanced sensitivity can be achieved by using AC techniques

[13]. In AC-AFM, the resultant interaction is a force gradient proportional to the measure frequency shift Δw of the force-sensing cantilever with a spring constant K_{stat}.

$$\Delta w = w(\frac{F'}{2K_{stat}}) \tag{3.1}$$

The fiber tip is glued to one of the tines of the tuning fork that is thus effectively our cantilever. The spring constant of our assembly (tuning fork/probe tip) is dominated by the geometry of the tuning fork (see later). Tuning fork's spring constant K_{stat} can be calculated and is given by $K_{stat} = (\frac{E}{4})W(\frac{T}{L})^3 \cong 26\times10^3 N/m$, where E is the elasticity modulus (i.e. Young's modulus) of the piezoelectric fork material, L is the length of the tube, T is the thickness and W is the width as indicated in Figure 3.3. The dimensions of the tuning fork are $3.5\times0.6\times0.25mm$. The tuning fork is vibrated in its anti-symmetric mode, without any motion of the its base in the direction of the two tines' vibration; therefor minimizing the dissipation energy (or, equivalently, maximizing its mechanical Q).

3.2 Implementation and Testing of Assemblies

3.2.1 Testing:

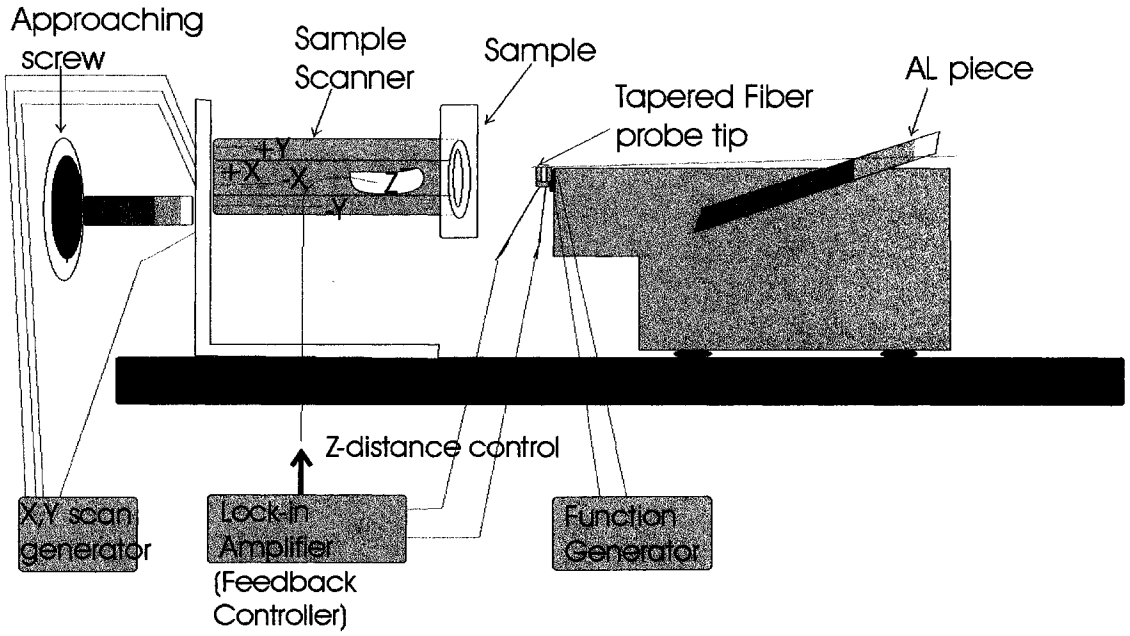

Figure 3.4 A schematic of tapping-mode test setup

Figure 3.4 schematically shows an experimental setup to efficiently and quickly evaluate our tuning fork/probe tip assembly of tapping-mode SNOM. A close-up of it is shown in Figure 3.3. In all assemblies, a commercially available crystal quartz tuning fork with resonance frequency of 32,768 Hz and Q factors of ~5,000 in air was used. A 15-cm tapered fiber tip is glued (with super glue) onto one of the tines of the tuning fork's.

This gluing of the fiber against the tuning fork is tedious but essential. The Q factor depends strongly on the gluing and can be dramatically degraded (from 5,000 to 350, see Figure 2.4 and Figure 3.5) by the possible migration of the glue along the tines of the fork.

The tip part of the fiber only extended 1 mm from the gluing point; it oscillates perpendicularly to the sample surface. When we first attached the fiber onto the tuning fork, no resonance frequency peak with reasonable Q factor (>100) was found.

When we used an aluminum metal piece to lift up the free end of the fiber, preventing it from touching the 2nd tine of the tuning fork, a resonance frequency peak with Q factor of around 300 (see Figure 3.6) was measured. We then replace the aluminum metal piece with some other items- a piece of cardboard, a Q-tip, a piece of plastic, Figure 3.7 is the resonance peak we obtained when we used a piece of cardboard to replace the aluminum metal piece. We can see that the resonance frequency peak has much lower Q factor (~ 100). We attribute this to the presence of more friction between the fiber and the surfaces for materials other than the metal surface, thus the energy dissipated more efficiently (lowering Q) when the fiber is vibrating. We concluded that the nature of how the free end of the fiber is mechanically constrained critically affects our system Q factor.

In the SNOM setup [14], the configuration of the probe assembly as well as the relative positions of the probe tip and sample are different from our test setup. Figure 3.8 depicts the details of the probe assembly in the SNOM under shear-force mode (a) and tapping-mode (b).

Instead of being epoxy glued to a piezoelectric oscillator, the tuning fork/probe tip assembly here is glued to a removable holder which is screwed to a 2.5-cm long dither piezo tube.

The dither piezo tube is epoxy glued to a 10-cm long aluminum shaft, which is connected rigidly to a fiber aligner. The whole probe assembly (with the dither piezo tube) sits inside a sample scanner – a 6.35-cm long, 1.27-cm outer diameter and 0.05-cm thick walled piezoelectric tube. While acquiring the data, the sample scanner is scanned with respect to the fixed probe tip. The fiber aligner adjusts the fiber to a proper position on the sample surface for scanning.

In order to implement tapping-mode in the SNOM setup, we replaced the tuning fork holder with a new one, which can hold the probe assembly in a way that it oscillates perpendicularly to the sample surface. (see Figure 3.8(b)). This configuration couldn't achieve the desired resonance frequency peak with reasonable Q factor (>200). A new inner tube is implemented (as depicted in Figure 3.9). Instead of connecting the tuning fork/fiber probe assembly to a dither piezo tube, the whole assembly is epoxy glued to a piezoelectric oscillator similar to the configuration of our tapping-mode SNOM test setup.

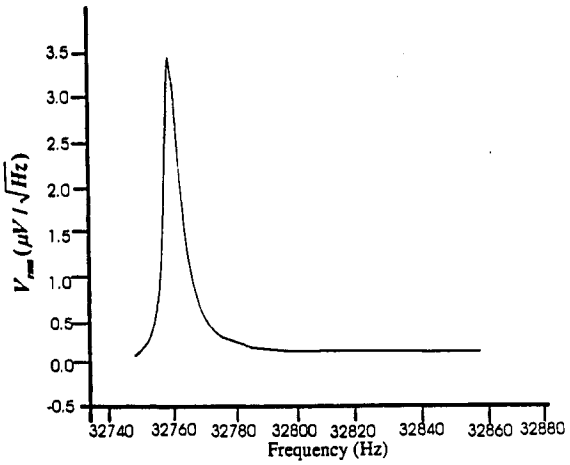

Figure 3.5 The resonance frequency of tuning fork/probe tip assembly (Q~350)

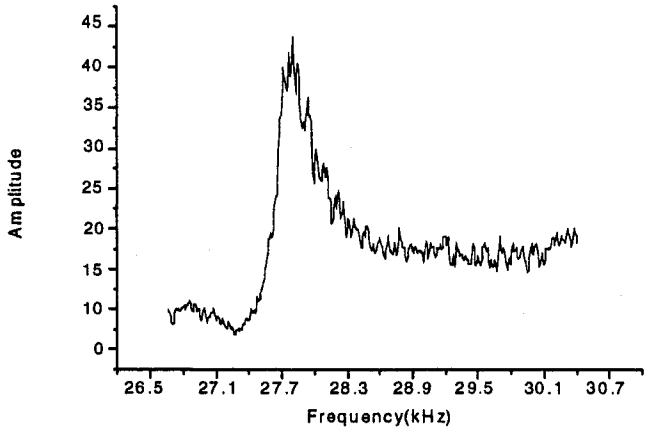

Figure 3.6 The resonance frequency peak for fiber being lifted up by Al Metal piece (Q~300)

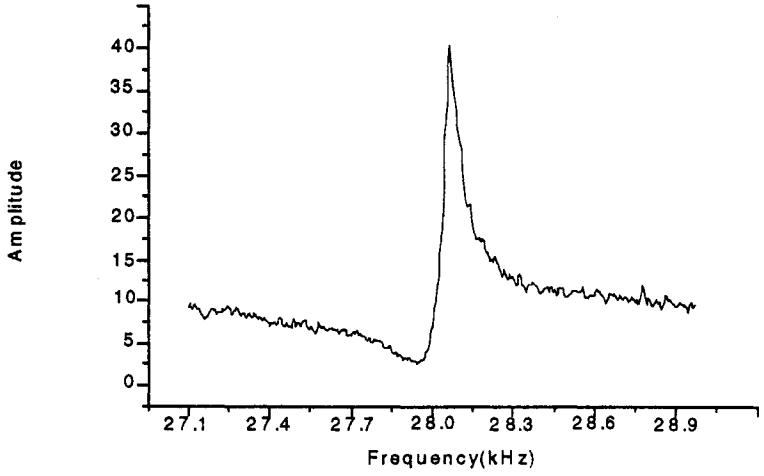

Figure 3.7 The resonance frequency peak for fiber being lifted up by cardboard (Q~100)

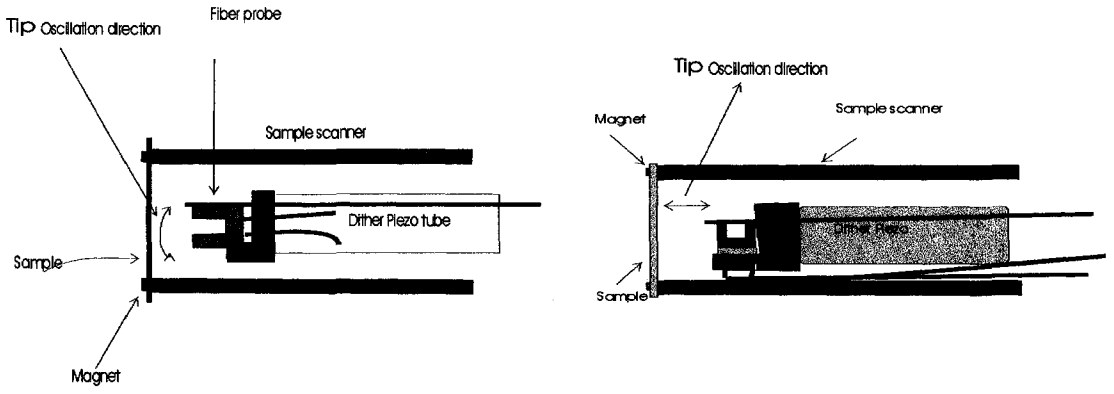

Figure 3.8 Probe assembly of (a) Shear-force (b) Tapping-mode SNOM

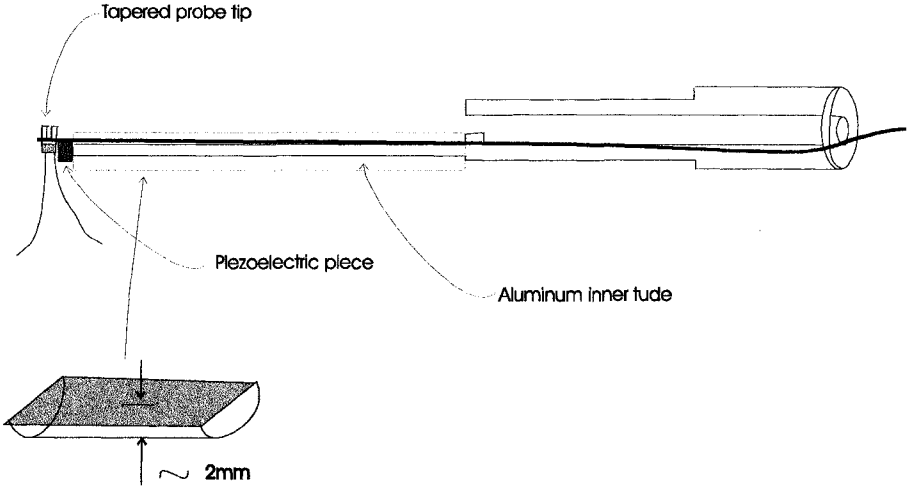

Figure 3.9 The revised version of inner tube of tapping-mode SNOM

An alternative way for implementing a tapping-mode fiber probe assembly is to attach only a few millimeters long tapered probe tip onto one tine of a tuning fork. This reduces the additional mass of one of the tines. Recall that the Q factor depends

strongly on the symmetry of the tines (Eq.(2.26)). Such an assembly has been reported in the literature [21], but has the problem of coupling light into the short attached fiber probe tip without excessive leakage. In passing we would like to mention that this 'tip-without-a-fiber' tuning fork assembly works well as a regular, non-optical force microscope, a property sometimes sought after in the imaging of e.g. light-sensitive quantum dots by AFM.

3.2.2 Results for Different Configurations

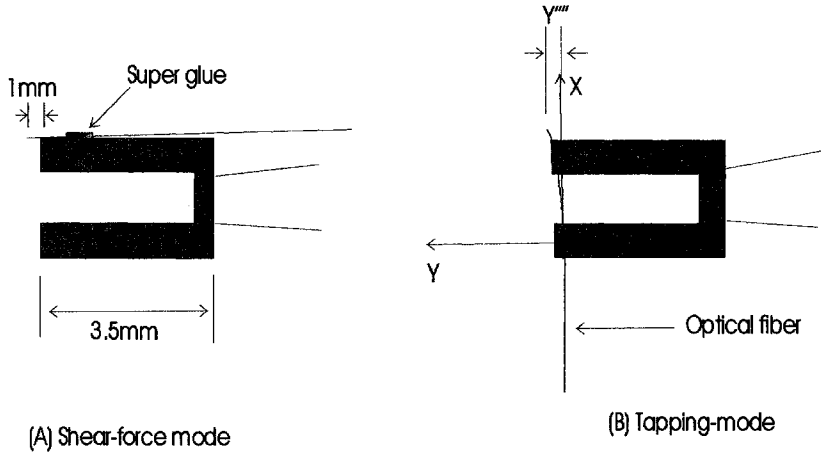

Figure 3.10 The tuning fork/probe tip assemblies of (a) Shear-force mode (b) Tapping-mode

The resonance frequency of the tuning fork/fiber probe tip assembly changes as the probe tip approaches the sample surface independent of the operation mode. In the following we investigate the effect of shear force and tapping mode configurations on the system Q factor. Recall that Q is one of the dominant factors determining the sensitivity of the measured force interaction.

3.2.2.1 The Shear-Force Configuration

A fiber is glued along the edge of a tuning fork's tine (see Figure 3.10(a)). Recall from Section 2.5.2, Eq.(2.26) [$\frac{1}{Q} = \frac{1}{Q_o} + \alpha \Delta f^2$] - the Q factor is dependent on the symmetry of the tuning fork's two tines - and Eq.(2.27) [$\frac{\Delta f}{f} = \frac{1}{2}(\frac{\Delta K}{K} - \frac{\Delta M}{M})$] - Δf (a mismatch between the resonance frequencies of tuning fork's tines) depends on the extra mass and stiffness due to the attachment of the fiber probe. When the tuning fork vibrates; the deformation of the fiber is a pure bending [15]:

$$\Delta K = \Delta K_{fiber} \approx \frac{\beta_n^4 E_f I_f}{L_f^3} \sim 1300 N/m$$

where E_f is the Young's modulus for the fiber material and I_f is the cross-sectional moment of inertia of the fiber $(I_f = \frac{1}{4} L^3 S)$, where L is the width of the fiber (~ the width of the tine), S is fiber cross-section. Considering a rectangular tine of width L and thickness t, $I_{tine} = \frac{1}{12} L^3 t$, if we assume the Young's modulus of the tuning fork and the fiber to be equal, we could get that both the mass (Δm) and the stiffness (ΔK) contributions the tine frequency mismatch are of the same order of magnitude- $\Delta K / K \cong 3\Delta M / M$. Also from Figure 3.3 and the dimensions of the tuning for $(3.5 \times 0.6 \times 0.25 mm)$, if we assume the densities of both the fiber and the tuning fork are the same, we can get:

$\frac{\Delta M}{M} = \frac{M_{fiber}}{M_{tine}} \cong \frac{1}{20} = \frac{2\Delta f}{f}$ for a 125-μm diameter and 4.5-mm long fiber attached to one of tuning fork's tines, with a measured resonance frequency mismatch Δf in our shear-force mode set-up of 750 Hz.

We thus expect (and also measured), from Eq. (2.26 &2.27), a Q factor of 800. We concluded that the reduction in Q (and thus sensitivity) is a result of the change in mass of the tine. A possible method to optimize Q would be by thinning the fiber, Thus reducing its mass.

3.2.2.2 The Tapping-Mode Configuration

This mode of operation is expected to be less destructive for both tips and samples, as only minimal normal forces act between tip and surface. It is implemented by placing a fiber across both tines of a tuning fork but attaching it to only one of them (see Figure 3.10(b)). In this configuration, when the deformation of the fiber is induced by the vibration of the tuning fork, it consists of not only the bending, but also the stretching/compression of the fiber. ΔK_{fiber} thus includes both a bending force constant (ΔK_b) and a stretching/compression force constant (ΔK_{sc}), which involves a far more complicated method for derivation. Ref.[21] derived the resulting formula for these bending and stretching/compression force constants of the fiber [15]:

$$\Delta K_b = (\frac{9}{175}) \times (\frac{\pi E y''^2}{L}) \times [\frac{1}{(1+\frac{9}{175}(\frac{y''}{d})^2)^2}]$$

$$\Delta K_{sc} = (\frac{\pi E d^2}{L}) \times [\frac{1}{(1+\frac{9}{175}(\frac{y''}{d})^2)^2}],$$

where y'' is the fiber displacement in the plane of tuning fork (when attaching the fiber to the tuning fork, it will inevitably have a certain degree of bending, as shown in Figure 3.10(b)). L is the length of the fiber probe tip (from the attaching point to the end of the tip, ~ 2.5 mm), and d is the fiber diameter. Supposed we have a straight fiber $(\frac{y''}{d} << 1)$, $\Delta K_{fiber} \approx K_{sc} \approx \frac{Ed^2}{L} \cong 10^5 N/m$ with a fiber probe tip of 125-μm diameter. This gives $\frac{\Delta K_{fiber}}{K_{stat}} \cong 10$, which means that the effective spring constant $(\frac{1}{K_{total}} = [\frac{1}{K_{tip}(=\Delta K_{fiber})} + \frac{1}{K_{\substack{tuning \\ fork}}(=K_{stat})}] \approx \frac{1}{K_{\substack{tuning \\ fork}}})$ of the assembly is dominated by the tine of the tuning fork. Thus, the extra mass loading $(\frac{\Delta M_{fiber}}{M_{tine}})$ still dominates the decrease of Q factor in tapping-mode.

We concluded that in tapping-mode, the Q factor should have a smaller dependency on the attachment of the fiber probe as in the shear-force mode. However, experimentally, we have great difficulty obtaining reasonable a Q factor (>200) in the tapping-mode configuration. This has to be due to the fact that there are other major

factors which also influence the Q factor; these include: the position of the gluing point of the fiber on the tuning fork, the amount of glue used and the natures of different glues used. All of these effects reduce the Q and thus the sensitivity of the SNOM. A larger minimal force interaction can in many cases lead to destructive imaging in tapping mode despite the expected benefits when compared to shear force detection. It has proven difficult to identify and control each factor and thus achieve tuning fork/probe tip assemblies with reproducible characteristics and high Q factor. An interesting observation is that the Q factor of shear-force assemblies ranged form 0 to 1000, while for tapping-mode they rarely exceeded 400.

Reconsidering Eq.(2.26 & 2.27), one should be able to observe that the unavoidable mass-loading ΔM (from the fiber probe) can be compensated by changing its spring constant ΔK. We tried to mount an identical optical fiber onto the other tine to compensate the different masses between two tines, however the Q factor has not been improved. The possible reason is that it is not easy to control the amount of the glue being used to attach the fiber to the tine, so adding equivalent mass to both of the tines is quite challenging to be achieved. One suggestion for future application is to modify ΔK by applying strain to the tuning fork. This changes the effective spring constant. As a result, one might be able (through careful tuning of the strain) to compensate for the frequency mismatch Δf between the tines and achieve a maximum Q.

3.3 Detecting Tip-Sample Interactions

The spring constants of our tuning fork/probe tip assemblies are high. Direct force measurements are thus not feasible if small forces of the order of nN are to be detected, as they would lead to undetectable small signals. AC techniques take advantage of resonant signal enhancement by a factor Q, leading to the possibility of detecting interactions that are small enough to be non-destructive.

It is well known in AC AFM that when the probe tip is within tens of nanometers of a sample surface, the amplitude, phase, and frequency of the probe assembly's vibration changes due to the interaction forces and force gradients between the fiber tip and the sample. Any one of the above parameters can be used as a feedback signal for tip-sample distance feedback control. There are several ways of demodulating the relevant parameters of the force sensor. One can measure the oscillation amplitude, frequency, phase or the piezo drive voltage necessary to maintain a constant oscillation amplitude. We investigated these techniques to find the optimal solution given the properties of our SNOM probe assemblies.

3.3.1 Lock-in Amplifier

The amplitude and the phase of the vibration of the probe assembly change as a result of the resonance frequency change. This can be seen from the equation of motion for a driven damped harmonic oscillator (our probe assembly) which is given by:

$$m_o \frac{\partial^2 \alpha}{\partial t^2} + (m_o w_o / Q)\frac{\partial \alpha}{\partial t} + m_o w_o^2 \alpha = F\cos(iwt) \ , \tag{3.1}$$

where $\alpha(t) = A_o \cos(wt + \theta)$.

From this one can calculate the amplitude and the phase of the probe assembly:

$$A = \frac{A_o (w_o / w)}{[1 + \theta^2 (\frac{w}{w_o} - \frac{w_o}{w})^2]^{\frac{1}{2}}} \tag{3.2}$$

and

$$\theta_o = \tan^{-1}[\frac{w_o w}{Q(w_o^2 - w^2)}] \tag{3.3}$$

From Eq.(3.2), the highest sensitivity is obtained at the largest slope; the optimal drive frequency (w) is thus:

$w \cong w_o(1 + \frac{1}{\sqrt{8}Q}) \cong 30{,}035\ Hz$ (in shear-force mode, with resonance frequency of about $30Hz$ and Q factor of about 350.)

At this drive frequency w, the amplitude and phase changes are related to the force gradient by the following expressions [22]:

$$\Delta A = (\frac{2A_o Q}{3\sqrt{3}K_{stat}})F' \tag{3.4}$$

and

$$\Delta\theta \cong \frac{w_o w F'}{2K_{stat} Q(w_o^2 - w^2)} \tag{3.5}$$

Experimentally, one determines the optimal driving frequency w by maximizing an amplitude change for a given frequency change Δw. The most commonly used

demodulator to detect the phase and amplitude changes for moderate Q factors is a lock-in amplifier. The probe assembly is driven with a piezoelectric oscillator at a fixed frequency w , which is also used as the lock-in reference signal.

3.3.2 Phase-Locked-Loop (PLL)

A Phase-Locked-Loop (PLL) [13,20] can be used to directly monitor either the resonance frequency shift (force gradient) or the Q factor (dissipation forces), both of which are influenced by the tip-sample interaction. Dissipative forces are measured by monitoring the amplitude of the piezo excitation signal necessary to maintain the amplitude of the oscillation constant when excited at resonance. A phase shifter in the PLL compensates for time lags (= system phase lags) in order to keep the correct phase between the driving signal and the response signal. An important part of the PLL is that the amplitude gain can have both positive and negative values, thus exciting or damping the probe assembly. This active damping leads to a substantial reduction in the ring-down time of the oscillation amplitude (given by $t_{response} = \frac{2Q}{w_o}$. However, in both shear-force mode and tapping-mode, the Q factor rarely exceeds 700. Ring-down times are thus typically 25 ms, which are comparable or smaller than typical pixel dwell time of 20 ms. Figure 3.11 and Figure 3.12 show the resonance frequency shift (constant Q mode) and Q factor change (constant frequency mode) of the probe assembly, respectively. In constant Q mode (Figure 3.11), we assume that

there is zero additional dissipation energy during imaging. The resonance frequency shift equation is given as [22]:

$$w_o' = (\frac{K_{stat} - F'}{m_o})^{\frac{1}{2}}, \tag{3.6}$$

assuming F' is much smaller than K_{stat}, which is the case of SNOM ($K_{stat} = 26{,}000N/m, F' = 10 \sim 30N/m$ from later derivation) and m_o is the effective mass.

First order expansion of Eq. (3.6) gives:

$$w_o' = w_o(1 - \frac{F'}{2K_{stat}}),$$

Therefore, in theory, if we assume the whole scanning process is in constant Q mode, we should have a resonance frequency shift of $(w_o' - w_o = 20Hz)$ for $F' = 10 \sim 30N/m$.

In the constant frequency mode (Figure 3.12), the relationship between the oscillation amplitude $A(w)$ and Q factor is given as :

$$A(w) = \frac{F_o / m_o}{\sqrt{[(w_o^2 - w^2)^2 + (w_o w / Q)^2]}} \tag{3.7}$$

By monitoring the drive amplitude changes at constant frequency $w \sim w_o$, one can extract the change in Q factor.

$$\frac{\Delta A}{A_o} \cong \frac{\Delta Q}{Q_o} \tag{3.8}$$

dissipation energy (only frequency shifts) or maximum dissipation energy (no frequency shifts). According to the expected values we derived above, in principle, one should be able to detect the tip-sample interaction with the given sensitivity of our PLL. However, SNOM has never successfully been operated in either constant Q factor mode or constant frequency mode with the PLL as a signal detector. The probable reasons are:

(1) Noise on the PLL input will reduce the frequency resolution of our PLL.

(2) The frequency shift of 20 Hz derived above is not a large dynamical range and easily leads to an unstable feedback.

(3) Instead of two extreme cases (Figure 3.11 – no dissipation energy and Figure 3.12 maximum dissipation energy), what's really happening during the scanning is actually the mixture of both cases, see Figure 3.13. Therefore, we have a smaller signal in both channels, which when combined with (1), leads to a SNR that is not useful for stable feedback.

In conclusion, one needs to improve the SNR of the tuning fork/fiber probe assembly signal in order to successfully use the PLL as a frequency detector.

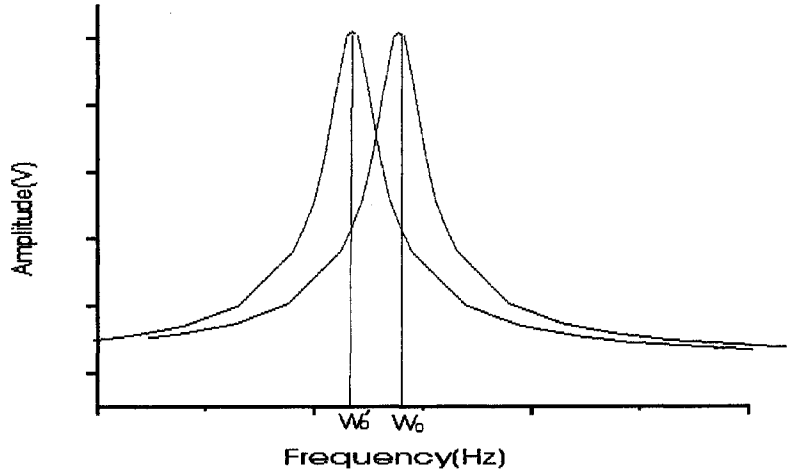

Figure 3.11 The resonance frequency shift during interaction zone

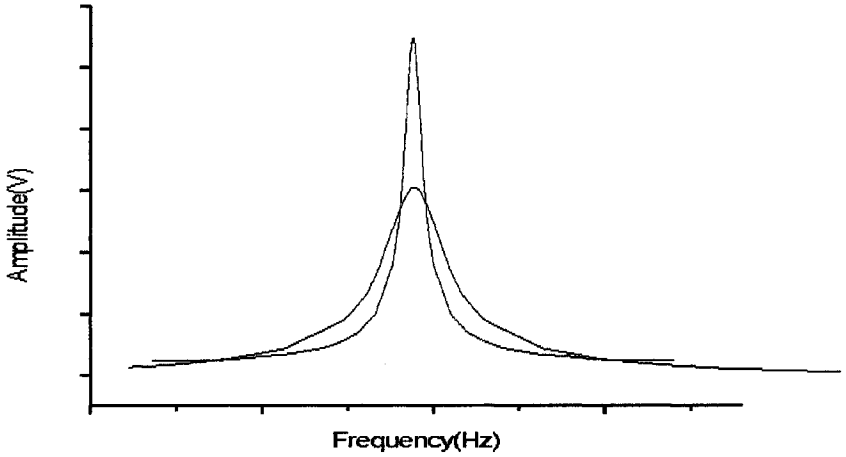

Figure 3.12 The Q factor change during the interaction zone

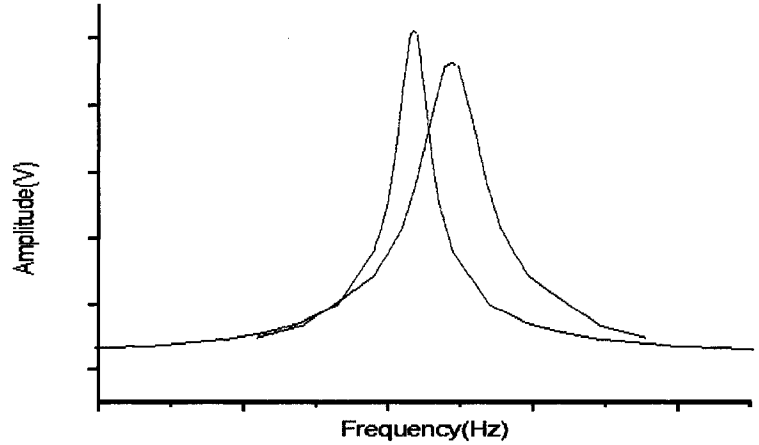

Figure 3.13 Both resonance frequency shift and Q factor change are expected for realistic interaction.

3.4 Experimental Results: Imaging

3.4.1 Feedback Distance Control (Force-Distance Curve)

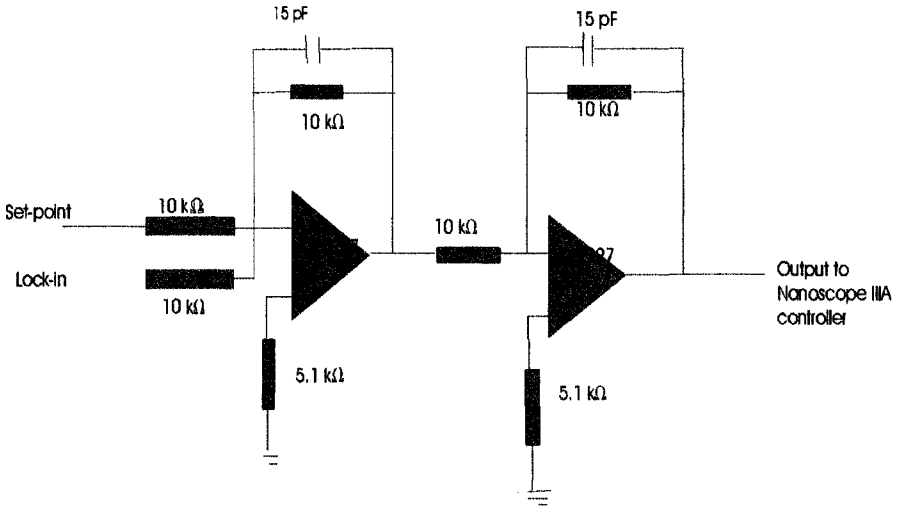

Figure 3.14 Schematic of the main control unit

Images are obtained with feedback control of the tip-sample separation. A crucial factor determining image quality is the choice of feedback parameters. The set-point controls the force interaction between tip and surface. A negative set-point voltage (approximately 85% of the free oscillation amplitude of the probe assembly) is added to the output signal from the lock-in amplifier (or PLL), and then sent to out main control unit, a Nanoscope IIIA controller from Digital Instruments. (see Figure 3.14). To prevent crashing the tip to the sample surface, the feedback reference value has to be set properly. If the set-point is set below 75% of the free oscillation amplitude, the tip-sample interaction would be too large, potentially damaging both tip and sample. A

smaller amplitude change than 85% would limit the dynamic range and stability of the feedback system.

Most of the SNOM groups use a set-point of around 85% of the oscillation amplitude to have the feedback operation in the real shear-force interaction zone. From this, we can get the value of force-gradient,

$$F' = \frac{\Delta A}{A_o} \times \frac{3\sqrt{3}K_{stat}}{2Q} \cong 10 \sim 30N/m, \tag{3.9}$$

where $\frac{\Delta A}{A_o} = 0.15$, $Q = 300$ and $K_{stat} = 26{,}000N/m$.

The Nanoscope software sends the amplified output signal ([$Signal_{Lock\text{-}in}$] + [Set-point value]) to the Z-piezo of the sample scanner tube to control the tip-sample separation. When the probe tip is close to the sample surface (< 10 nm), the interaction force between tip and sample reduces the oscillation amplitude of the probe assembly, so the output signal becomes negative, and the sample scanner tube is extended (away from the tip). When the oscillation amplitude increases, the output signal becomes positive and the scanner tube is retracted (towards the tip).

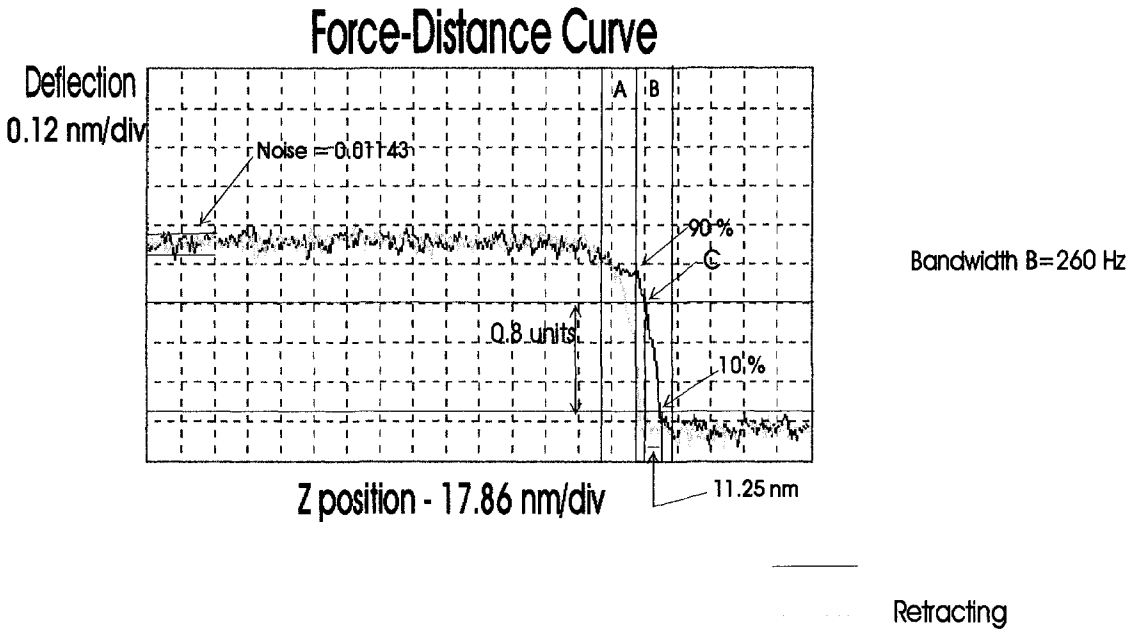

Figure 3.15 Force-Distance Curve for Shear-force mode SNOM

From Figure 3.15, we can see that there are two interaction zones - A and B. In the first interaction zone (A), the tip is still far away from the sample surface (~ 35 nm); the sudden drop of the amplitude could be due to a surface "contamination" layer [23], which in the cases of hydrophilic sample surfaces consist of water. When the tip is at a distance within 10 nanometers from the sample surface (zone B), the probe tip starts to interact with the sample. Point C marks the operation point of the feedback circuit. In this case, the signal to noise ratio (SNR) is around 70 (0.8 units/0.01143units); the possible sources for the noise are the input noise of the lock-in amplifier and stray capacitance. The former noise source is about 96.7 nV (from the lock-in amplifier manual), which is only 1.6% (96.7nV/6μV) of the measured signal amplitude. We thus conclude that the main source of the noise comes from the variations of the stray

capacitance. The presently advanced SNR is however sufficient to gives us a distance resolution of around 0.16nm ($\frac{\Delta x(11.25nm)}{SNR}$) in a tip-sample interaction zone of 11nm.

3.4.2 Images

In the following, some images are shown to examplify some of the encountered problems with shear-force and tapping-mode operations of the SNOM tips.

3.4.2.1 Images of CD stamper

Figure 3.16 shows the images of CD stamper taken under (a) SNOM tapping-mode (c) SNOM shear-force mode and the expected shape of a CD stamper image taken under (e) Scanning Electron Microscope (SEM). The SNOM images (a) and (c) were taken at a scan rate of 0.1 Hz and are comprised of **512×512** data points.

Plots (b) and (d) are the cross-section along the black lines on each image. In the tapping-mode image (a), we can see the wiggling lines in the whole image; it also shows in the cross-section plot (b) (the noise of the plot), it is due to the unproper proportional gain while we scanned the CD stamper. We found it very difficult to optimize feedback settings of tapping-mode SNOM due to a small phase space for stable operation.

In the shear-force mode image (c), one observes two identical features appearing right next to each other, which is the result of a classical artifact: a double tip (see Figure

3.17). Double tips are difficult to avoid, as the topography is quite rough and feedback errors can easily lead to shearing off of a fragile glass tip. This often leads to double tips. The appearance of this type of artifact is easily noticed on a calibration sample, but can be more difficult to notice on soft samples. We would like to point out that tapping-mode operation is much less susceptible to fracturing of the SNOM tips.

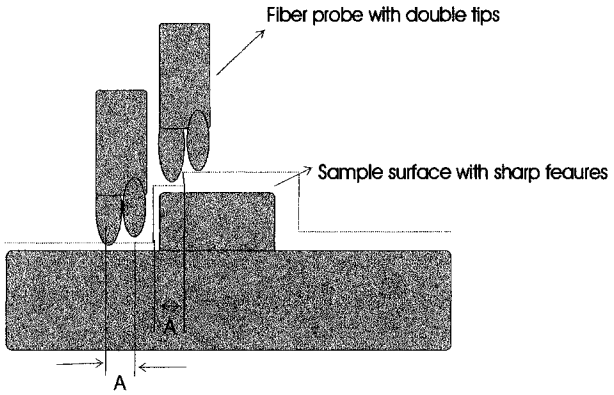

Figure 3.17 The double-tip effect on sample topography

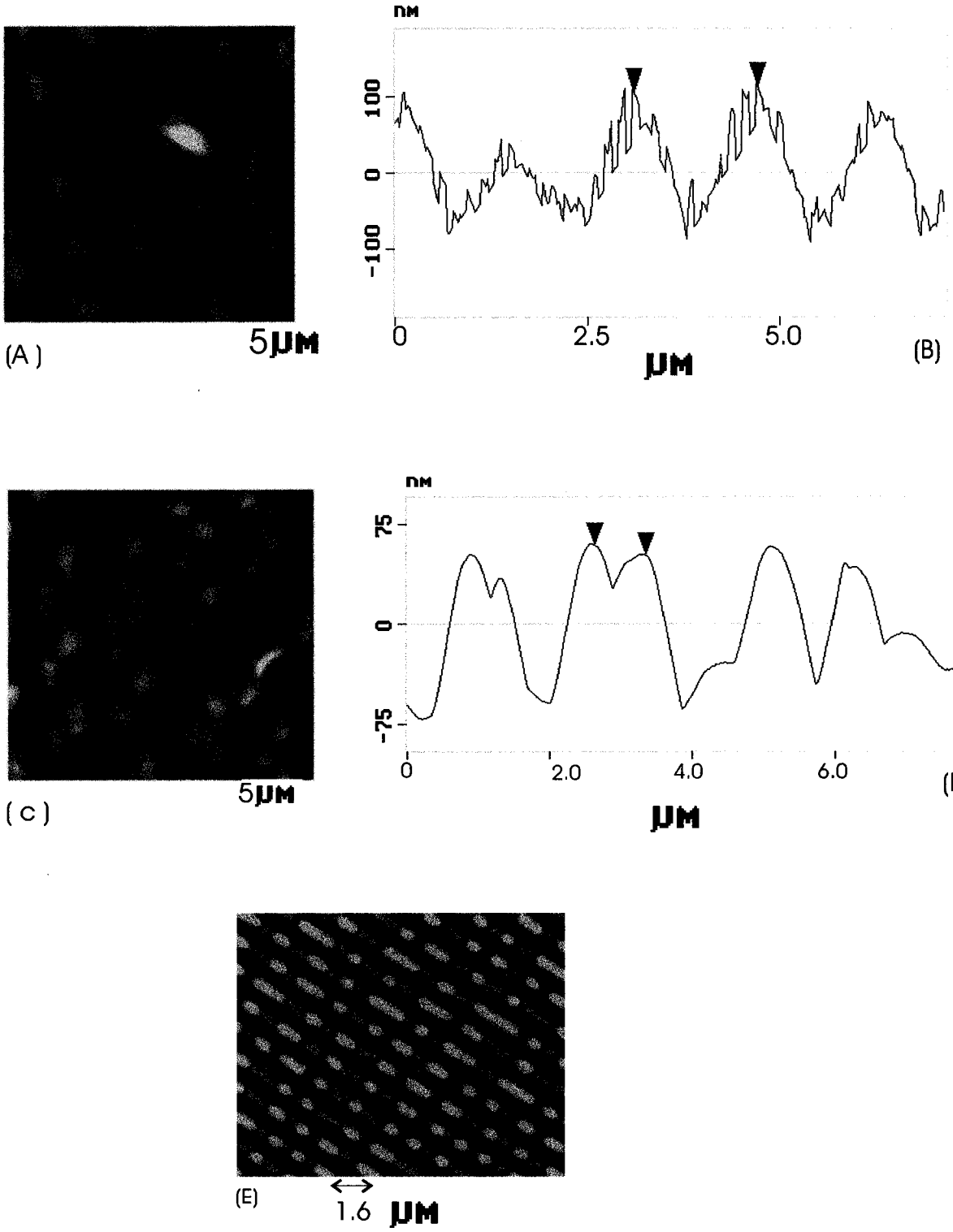

Figure 3.16 (a) The image of CD stamper under Tapping-mode ;with its cross-section analysis (b)
(c) The image of CD stamper under shear-force mode; with its cross-section analysis (d)
(e) The image of CD stamper under AFM

3.4.2.2 Images of Polystyren

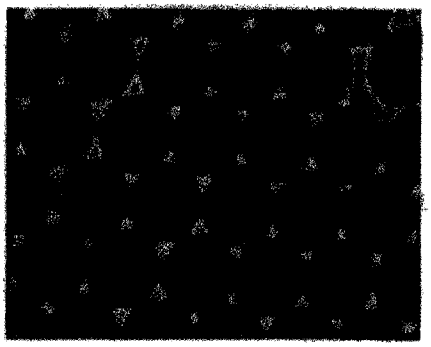

Figure 3.19 The Polystyrene image taken under SEM. From [1]

The polystyrene sample is prepared as the following procedures: deposit the polystyrene latex microspheres as close-packed monolayer on a glass coverslip then coat the layer with a thin film of metal. Once the polystyrene is dissolved, a regular array consisting of sub-micron sized metal triangles remains on the coverslip. It shows hexagonal symmetry. The spheres between them are one micron in diameter [14]. Figure 3.18 shows the close-packed monolayer of polystyrene microspheres image taken under the SEM; it shows hexagonal symmetry.

Figure 3.19 is the polystyrene image taken under shear-force SNOM for three different scan sizes of (a) 5.99μm (b) 10.5μm (c) 20.0μm. Figure 3.20 is the same polystyrene sample taken under tapping-mode SNOM for scan sizes of (a) 12.8μm and (b) 20μm. Both of the tapping-mode and shear-force mode images show the hexagonal symmetry (see the drawn hexagon on each image).

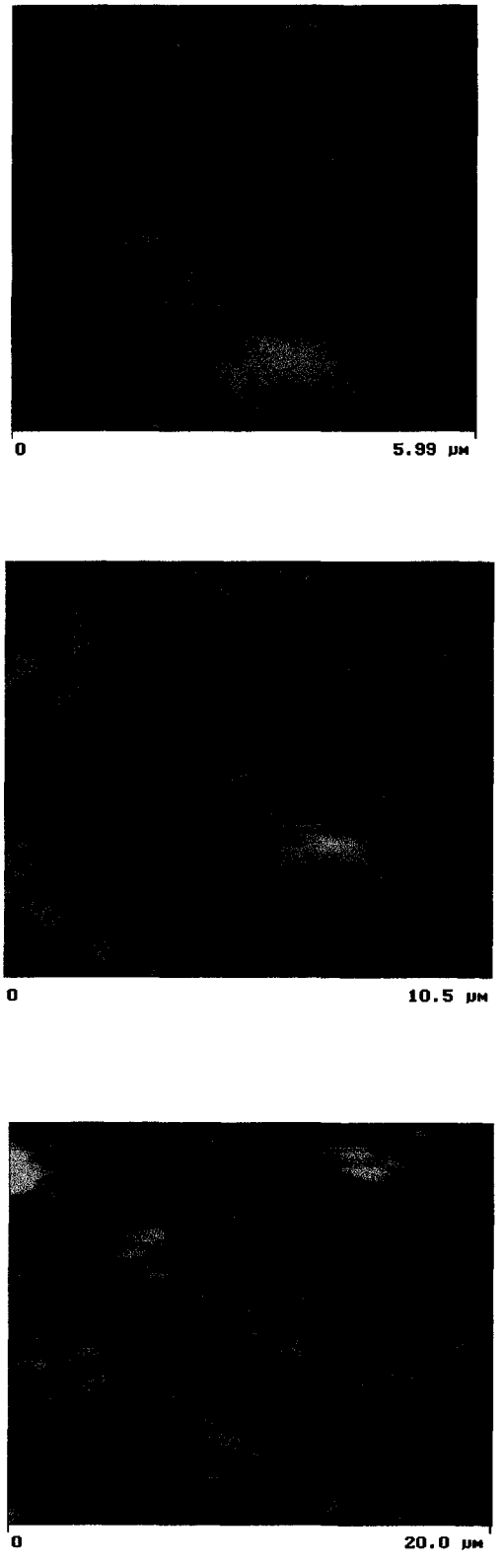

Figure 3.19 Polystyrene images under shear-force mode of three different scan size (a) 5.99 (b) 10.5 (c) 20.0

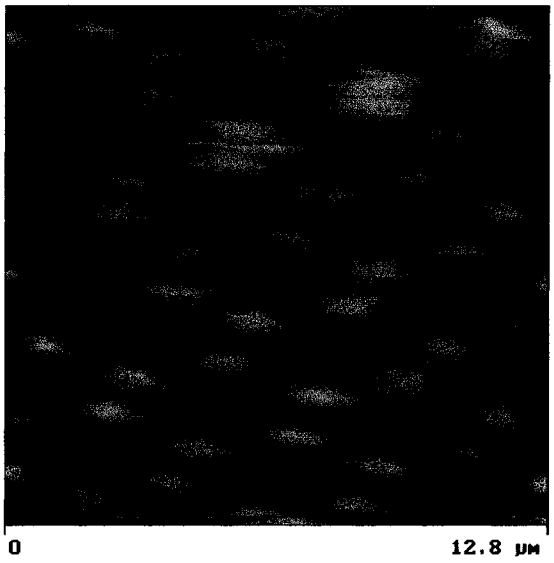

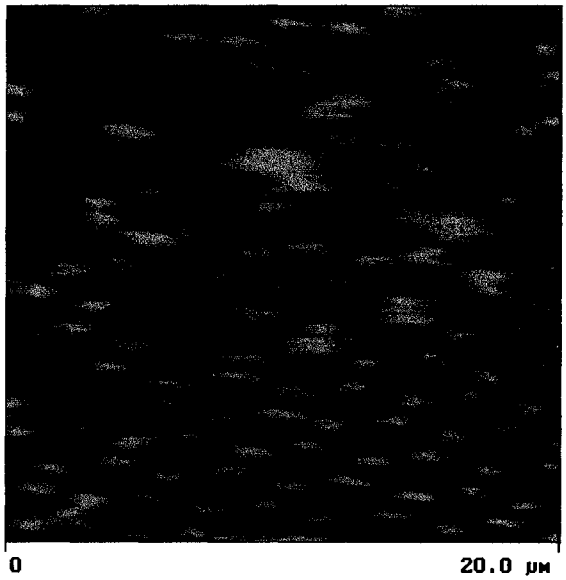

Figure 3.20 Polystyrene images taken under tapping-mode of two different sizes (a) 12.8 (b) 20.0

In the images taken under both operation modes, round blobs were imaged instead of sharp triangles. However, they do exhibit the correct hexagonal symmetry, so it is evident that a blunt tip was used. Figure 3.21 explains how a blunt tip affects the sharp features of sample topography.

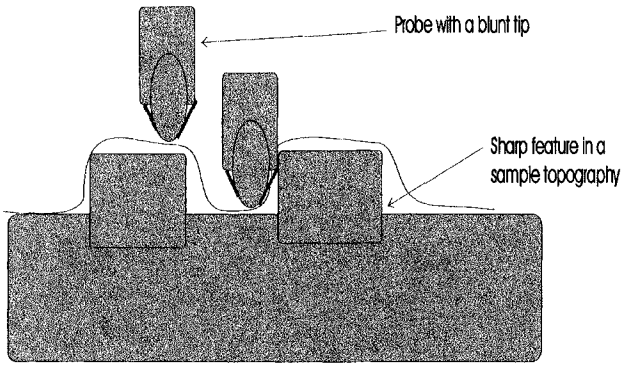

Figure 3.21 The effect of a blunt tip scans over a sharp feature of a sample surface

In the tapping-mode images, although the hexagonal symmetry was still shown, it is much less well defined as compared to its shear-force counterparts. We attribute this to a frequent loss of the feedback signal when tracking the sample surface. The tip then just oscillates freely, not measuring any tip-sample interactions until the feedback "finds" the surface again. We finds that the small dynamical range of the feedback system of tapping-mode is a major limitation of using this method for tip-sample distance control. The small Q factor of tapping-mode, which rarely exceeds 400 (these two images were taken under Q factor of a value of < 200), leads to a poor sensitivity and signal to noise ratio (SNR), both of which do not help the stable feedback operations.

3.4.2.3 Summary

CD stamper and Polystyrene images were taken under tapping-mode and shear-force mode SNOM. In comparison to the images of Scanning Electron Microscope (SEM), they show the same symmetry. In most of the images, artifacts were encountered; it was a result of the convolution of a blunt probe tip with the sample as well as the feedback settings, which cause the stable operations extreme difficult.

As far as the images were concerned, we concluded that the implementation of tapping-mode SNOM would provide an alternative operation mode if more stable feedback operation can be implemented. This can only be achieved if the input signal SNR is increased. The most dominated factor is to improve the Q factor of the tuning fork/probe tip assembly.

Tapping-mode SNOM is not yet ready for routine operations; difficulties were occurred during the tapping-mode scanning. As a result, not many successful images were taken, which leads to insufficient information for more thorough data analyzing. By optimizing all the parameters affecting the operations, one will expect a more stable and routine operation for acquiring more qualifying images. A further investigation will then be made possible to enable one to have a successful tapping-mode implementation.

Chapter 4

Conclusion and Outlook

Scanning Near-Field Optical Microscopy (SNOM) is an excellent tool to optically investigate surface properties beyond the classical limit, and it is in principle suitable for application in the life sciences. The use of force feedback in SNOM allows one to obtain additional information about the sample surface. It also allows for the simultaneous acquisition of topographical and optical images. The essential elements of a force-detection system are a quartz tuning fork and an optical fiber probe. The tuning fork acts as a force sensor, while the fiber probe tip acts as a force pick-up and defines the optical near-field aperture.

For this project, tapping-mode feedback is implemented and investigated. Those factors which influence the performance of tapping-mode SNOM and make the routine operation very challenging were discussed. In summary, we conclude that:

1. The implementation of tapping-mode:

The implementation of tapping-mode is challenging due to the easy and not well understood reduction of the mechanical Q factor of the tuning fork/probe tip assembly configuration (Section 3.2) [18], and to the necessary confined geometrically configuration of the SNOM setup [14].

1.1 The comparable dimensions of the tuning fork and the fiber probe makes the gluing tedious and difficult [24]; different glues used were strongly affecting the coupling between the tuning fork and the fiber probe as well as the reproducibility of the gluing itself.

2. In the tuning fork/probe assembly, the unavoidable mass loading (fiber probe and the excess of glue used) breaks the symmetry of tuning fork's two tines, which dramatically reduces the Q factor and consequently affects the sensitivity of the operation.
3. Stray capacitance of the tuning fork [25] and external electronic devices reduce SNR of the feedback input signal.
4. The difficulty of adjusting suitable feedback parameter settings, due to the small dynamic range allowing stable feedback operations, can be observed from the CD stamper and Polystyrene images taken under tapping-mode SNOM.

To sum up, in principle, SNOM under tapping-mode is expected to generate better sensitivity and stability. Almost no lateral force involved during operation greatly reduces the chance of damaging both the probe tip and the sample surface, which is essential for biological and soft samples. However, among all the factor which degrade the performance of tapping-mode SNOM, it is not easy to investigate each one of them without affecting the rest. The applicability of living cells in tapping-mode under current SNOM condition is not yet practical as the contact of probe assembly to the aqueous solution will further degrade the Q factor.

Future investigations should be focused on the improvement of the signal to noise ratio (SNR) of the tuning fork/probe tip assembly signal. This can be done by the

following methods: (a) Investigate the origin of the reduced Q factor in the tapping-mode compared to the shear-force assemblies. Remember that theoretically both tapping-mode and shear-force mode probe assemblies should show the same reduction in Q factor. Empirically, tapping-mode assembly leads to inferior Q factor. (b) An implementation of a pre-amplifier close to the probe assembly to enhance the signal (c) Using the piezoelectric tuning fork as a oscillator by building a I-V converter box [25] which directly drives the tuning fork with a resonance voltage and the induced current can be measured. This can remove the need of an additional piezoelectric oscillator; thus reduce the external stray compacitance. (d) Placing the whole probe assembly into a vacuum environment (many other microscopes are operated under vacuum condition) to further reduce the external influence.

By improving the SNR of the probe assembly, it will allow successful implementation of a PLL, with which one can further investigate the origin of tip-sample interaction force. Better SNR will also make stable feedback control possible.

BIBLIOGRAPHY

[1] U. Dürig, D. W. Pohl, and F. Rohner, *J. Appl. Phys.* 59, 10 (1986)

[2] K. Wang, X. Wang, N. Jin, W. Huang, and J. Xu, *Journal of Microscopy* 194, 317 (1999)

[3] A. Dräbenstedt, J. Wrachtrup, and C. von Borczyskowski, *Appl. Phys. Lett.* 68, 10 (1996)

[4] J. Barenz, O. Hollricher, and O. Marti, *Rev. Sci. Instrum.* 67, 5 (1996)

[5] Th. Röder and L. Paelke *et al. Rev. Sci. Instrum.* 71, 7 (2000)

[6] Shmuel Shalom, Klony Lieberman, and Aaron Lewis, *Rev. Sci. Instrum.* 63, 9 (1992)

[7] J-K Leong and C.C. Williams, *Appl. Phys. Lett.* 66, 11 (1995)

[8] Khaled Karraï, Robert D. Grober, *Ultramicroscopy* 61, 197 (1995)

[9] Hagen Göttlich and Robert W. Stark, *Rev. Sci. Instrum.* 71, 8 (2000)

[10] R. Brunner, O. Hering, O, Marti, and O. Hollricher, *Appl. Phys. Lett.* 71, 25 (1997)

[11] Levi A. Gheber, Jeeseong Hwang, and Michael Edidin, *Applied Optics* 37, 16 (1998)

[12] Michael A. Paesler, and Patrick J. Moyer, *Near-Field Optics* (1996)

[13] E. Betzig, M. Isaacson, and A. Lewis, *Appl. Phys. Lett.* 51, 25 (1987)

[14] P. LeBlanc, Dual-Wavelength Scanning Near-Field Optical Microscopy, Ph.D. Thesis McGill University (2001)

[15] Konstantin B. Shelimov, Dmitri N. Davydov, and Martin Moskovits, *Apply. Phys. Lett.* 75, 2 (1999)

[16] Din Ping Tsai and Yuan Ying Lu, *Appl. Phys. Lett.* 73, 19 (1998)

[17] Anders Kühle, Alexis H. Sørensen, and Jakob Bohr, *J. Appl. Phys.* 81, 10 (1997)

[18] Javier Tamayo, *Appl. Phys. Lett.* 75, 22 (1999)

[19] T. Sulchek, R. Hsieh, J. D. Adams, G. G. Yaralioglu, S. C. Minne, and C. F. Quate, *Apply. Phys. Lett.* 76, 11 (2000)

[20] G. T. Shubeita, S. K. Sekatskii, B. Riedo, and G. Dietler, *J. Appl. Phys.* 88, 5 (2000)

[21] C. Höppener, D. Molenda, H. Fuchs, and A. Naber, *11th International Conference on STM* (2001)

[22] P. Grütter, H. J. Mamin and D. Rugar, *Scanning Tunneling Microscopy II* 28, 15 (1992)

[23] J. U. Schmidt, H Bergander, and L.M Eng, *J. Appl. Phys.* 87, 6 (1999)

[24] J. Salvi, P. Chevassus, A. Mouflard, S. Davy, M. Spajer, and D. Courjon, *Rev. Sci. Instrum.* 69, 4 (1997)

[25] Robert D. Grober, Jason Acimovic, Jim Schuck, Dan Hessman, Peter J. Kindlemann, Joao Hespanha, and A. Stephen Morse, *Rev. Sci. Instrum.* 71, 7 (2000)

[26] Walid A. Atia and Christopher C. Davis, *Appl. Phys. Lett.* 70, 4 (1997)

[27] Bert Hecht, *Forbidden Light Scanning Near-Field Optical Microscopy* (1996)